Electronic Supplementary Material (ESI) for Physical Chemistry Chemical Physics.

Supplementary Information for "Multichannel Photodissociation Dynamics in CS_2 Studied by Ultrafast Electron Diffraction"

Weronika O. Razmus, Kyle Acheson, Philip Bucksbaum, Martin Centurion, Elio Champenois, Ian Gabalski, Matthias Hoffman, Andrew Howard, Ming-Fu Lin, Yusong Liu, Pedro Nunes, Sajib Saha, Xiaozhe Shen, Matthew Ware, Emily M. Warne, Thomas Weinacht, Kyle Wilkin, Jie Yang, Thomas J. A. Wolf, Adam Kirrander, Russell S. Minns, and Ruaridh Forbes

1 Calculation of $\Delta\mathrm{PDF}(R,t)$

In ideal cases, the relative changes in the pair distribution function (PDF) upon excitation gives access to a real space analysis of the nuclear wavepacket in terms of changes in the internuclear distances. This can be calculated as a sine transform of the difference molecular function, $\Delta\mathrm{sM}(s,t)$, which is calculated from the experimental data as,

$$\Delta\mathrm{sM}(s,t) \approx s\frac{I(s,t)-I(s,t\ll 0)}{I_{\mathrm{at}(s)}}, \tag{1}$$

where s is the momentum transfer, t the delay time, and $I(s,t)$ and $I(s,t\ll 0)$ the signal at times t and $t\ll 0$, i.e. the latter is the reference signal before excitation by the pump pulse. Finally, $I_{\mathrm{at}}(s)$ is the static atomic background that results from the incoherent sum of the scattering from the individual atoms.

We can convert the measured scattering pattern from reciprocal space s to real space R in order to obtain the difference pair distribution function, $\Delta\mathrm{PDF}(R,t)$. This shows how the distribution of interatomic distances, R, changes over time. It is achieved through the application of a sine transform as follows,

$$\Delta\mathrm{PDF}(R,t) = \int_{s_{\mathrm{min}}}^{s_{\mathrm{max}}} \Delta\mathrm{sM}(s,t)\sin(sR)\mathrm{e}^{-\alpha s^2}ds, \tag{2}$$

with ideally $s_{\mathrm{min}}=0$ and $s_{\mathrm{max}}=\infty$, although in practice the experimental range will be smaller. At the very least, some data at small s will be missing where the direct (unscattered) electron beam passes through a hole in the detector. The exponential damping function, $\exp(-\alpha s^2)$, is included to minimise high-frequency artefacts from the truncation of the signal at s_{max} by smoothly reducing the intensity of the measured signal towards zero at $\mathrm{s_{max}}$. As discussed below, the high-s signal can be more noisy and the α parameter can be tuned to reduce the contribution from the noise. At the lower end of the range, for $s<s_{\mathrm{max}}$, linear extrapolation of the experimental signal to $s\to 0$ can be used if only little of the signal is missing. When calculating the $\Delta\mathrm{PDF}(R,t)$ from simulations, the range of s is of course not limited.

1.1 Comparison of ΔsM_{exp} and ΔsM_{th}

Figure S1 shows the experimental $\Delta sM_{\mathrm{exp}}(s,t)$ and the $\Delta sM_{\mathrm{th}}(s,t)$ derived from the theory. The first thing to note is that the experimental signal is quite noisy. In part, this is because some of the error cancellation present in the percent difference signal, $\%\Delta I_{\mathrm{exp}}(s,t)$, is absent. The reason for this is that the denominator in the $\%\Delta I_{\mathrm{exp}}(s,t)$ is taken from the experimental data, while the $I_{\mathrm{at}(s)}$ is *not* a quantity measured experimentally. However, looking at Fig. S1, it is apparent that the noise is greatest at larger values of s. This relates to the s^{-4} damping inherent in the differential cross section for electron scattering, which arises from the modulation of the scattering amplitude by the Rutherford cross-section. This in turn leads to poorer statistics at high values of the momentum transfer s. The signal at negative times in particular, the top panel in Fig. S1 and Fig. S2, give a sense of the noise levels.

Comparison of the theoretically calculated ΔsM_{th} signal and the experimental data in the small-s region, $s\leq 1$ Å^{-1}, shows that the experimental data misses anticipated modulations in the ΔsM signal, as seen in Fig. S1 and Fig. S2. The small-s region is not quite resolved in the experiment due to the limited detection range and a combination of centre-shifting and streaking resulting from e.g. plasma effects. The small-s differences between the theoretical and the linearly extrapolated experimental ΔsM are sufficient that the ΔPDF derived from experimental data is not reliable, as we shall see.

As an aside, we finally note that the presence of the damping function significantly reduces the impact of the large-s noise in the experimental data. This is illustrated by the inclusion of the damped $\Delta sM_{\mathrm{exp}}(s,t)\exp(-\alpha s^2)$ curve (dashed green) in Fig. S1 and the panel b) of Fig. S2, with $\alpha=0.035$. The rather steep damping does reduce the intensity of signal in the intermediate s range where much of the structural information lies.

In the next section, we examine the consequences of the differences between the $\Delta sM_{\mathrm{exp}}(s,t)$ and the $\Delta sM_{\mathrm{th}}(s,t)$ for the ΔPDF.

1.2 Examining the ΔPDF

In Fig. S3 we show the ΔPDF at the same delay times shown for ΔsM in Fig. S1. The corresponding heatmaps can also be seen in Fig. S4. It is clear that the ΔPDF that results from the experimental ΔsM_{exp} is shifted upwards relative the theoretical counterpart and that a broad shoulder is present at atomic distances of less 1Å. These

features in the experimental $\Delta\text{PDF}_{\text{exp}}$ are unphysical as they imply extremely short distances not expected to appear during the dynamics, as well as a permanent increase at large t of bond lengths at intermediate distances that again are not to be expected during this reaction. In contrast, the theoretical $\Delta\text{PDF}_{\text{th}}$ shows the anticipated depletion of C−S and S−S bond lengths without any persistent increase in intermediate distances, but rather the expected *transient* increases, as seen in the main manuscript.

Crucially, if one truncates the size of the transform window in order to exclude theoretical data in the range $s \leq 1$ Å^{-1}, which is absent in the experimental data, the resulting $\Delta\text{PDF}_{\text{th}}$(truncated) reproduces the observed experimental Δ PDF$_{\text{exp}}$ as seen in Fig. S3. This implies that the absence of experimental data for $s < s_{\text{min}}$ limits the validity of the experimental ΔPDF_{exp}. Finally, from a mathematical point of view, the lack of signal at low s in the ΔsM_{exp}, where the scattered wavelets all scatter in phase in the limit of $s \to 0$, amounts to the exclusion of low frequencies in the sine transform, which does explain why the experimental $\Delta\text{PDF}_{\text{exp}}$ is shifted by a nearly constant term.

1.3 ΔsM_{exp}, $s\Delta I_{\text{exp}}$, and $\%\Delta I_{\text{exp}}$

The first point of note is that while, in the current case, the lack of low s data inhibits the real-space interpretation of the experimental data in terms of an $\Delta\text{PDF}_{\text{exp}}$ derived directly from the ΔsM_{exp}, it does not preclude the momentum space analysis carried out in the manuscript since the trajectory fitting procedure uses the $\%\Delta I_{\text{exp}}$ signal across the usable range of s, without any truncation effects and with the additional benefit of lower noise due to further noise cancellations.

One could also pose the question if it might be possible to approximate the ΔsM_{exp} by an approximate $\Delta sM_{\text{approx}}$ defined as

$$\Delta sM_{\text{approx}}(s,t) \approx s\Delta I_{\text{exp}} = s\frac{I_{\text{exp}}(s,t) - I_{\text{exp}}(s,t \ll 0)}{I_{\text{exp}}(s,tt \ll 0)}. \tag{3}$$

The utility of this approximation for ΔsM_{exp} can be examined using theoretical data, for which we define

$$\Delta sM_{\text{th,approx}}(s,t) \approx s\Delta I_{\text{th}} = s\gamma\frac{I_{\text{th}}(s,t) - I_{\text{ref}}(s)}{I_{\text{ref}}(s)}, \tag{4}$$

where γ is the excitation fraction and I_{ref} the time-independent ground-state reference scattering. A comparison of the $s\Delta I_{\text{th}}$, i.e. the approximation above, and the ΔsM is shown in Fig. S5. The differences are strongest at the small values of s, shown above to have an effect on the ΔPDF. These differences can be explained by the difference in the total scattering term of the ground state Wigner distribution in comparison to the geometry independent atomic scattering term. These two terms amount to the different denominators used in the calculation of the $\%\Delta I$ and ΔsM signals. Fig. S6 shows the ratio of these two terms, it is clear that the biggest difference is at $s \leq 1.5$ Å^{-1}, which is where the biggest discrepancy in Fig. S5 is present. Following the low s region there are then a series of successive oscillations that shrink in magnitude, these are clearly correlated with the discrepancies seen at the extrema of Fig. S5.

Finally, in Fig. S7 it is evident that the optimisation of the trajectories in the space of $\%\Delta I$ also improves the quality of the signal in the space of ΔsM. Hence showing that we have converged to a global minimum and that the optimisation algorithm is robust.

2 Validity of Optimisations

In order to visualise differences in the experimental and the theoretical signal that results from the optimisation procedure outlined in the main text, we plot the RMSD for each time delay over a series of subsets of regions in the total momentum transfer range. Heatmaps of the experimental and optimised and unoptimised theoretical signal, can be seen in Fig. S8. Here we refer to the optimised theoretical signal as the signal resulting from the optimisation with free parameters $(\gamma, \Delta t, \tau_c) = (3.40\%, -83, 230)$ fs, this fit corresponds to a global RMSD of 0.69 and a global RAE of 0.88. It may be difficult to observe details in heatmaps as they are prone to hiding information, but there are some broad trends that can be seen here. Qualitatively, one can see that the theoretical signal reproduces the main features of the experiment across all time steps. In the main text we highlight the discrepancy in the fit at timesteps around 150 fs and at $s = 4.4 - 5$ Å^{-1}, this can be seen in the RMSD plot shown in Fig. S9 as a sharp peak at 150 fs for the subset of $s \in [4.3, 6.3]$. Generally, it seems that the experimental signal observes a slightly stronger depletion region around 5 Å^{-1} across time. In addition, one can see that around 8 Å^{-1} the theoretical signal predicts a slightly more intense peak at $s = 8$ Å^{-1}. The higher discrepancy between the experiment and optimised theory here is reflected in the RMSD of the two higher momentum transfer regions. This is somewhat expected given the s^{-4} scaling which results in poorer statistics and a greater degree of noise. Below $s = 4$ Å^{-1} the discrepancy in intensity is less and the signals match well in the region where the majority of the structural information lies. The performance of the optimisation here is shown by the RMSD over time for the subset of $s \in [1, 4.3]$. In the low to intermediate s range the RMSD is low and varies little in time.

In comparison the two second best optimisations correspond to free parameters $(\gamma, \Delta t, \tau_c) = (3.61\%, 16, 230)$ fs and $(3.74\%, 34, 230)$ fs respectively. These two sets of values resulted in a RMSD of 0.69 and 0.70, and also a RAE of 0.89 and 0.90. While the global RMSD in these two cases is similar to the best optimisation, one can confirm the best result by the RAE and the result of the independent t_0 fit.

3 Signal Decomposition and Inferred Dynamics

As discussed in the main text, the delayed enhancement seen just below 2 Å^{-1} is indicative of dissociation. As expected, this feature emerges at earlier times in the rapid singlet dissociation channel, whereas there the onset of the triplet contribution is delayed by a greater amount due to the nature of ISC. Fig. S10 shows the intensities of the centres of the peaks that correspond to this dissociative signal. It is clear the main rise in the singlet contribution to the theory is at early times, and the triplet contribution at later times. At around 500 fs the singlet signal levels off to value that is almost constant in time as here the contribution is from the remaining longer lived singlet dissociative states. While there is overlap with the triplet channel over all time delays, the majority of the singlet dissociation occurs at earlier times and the triplet on average, occurs at later times. This is reflected in the slower onset of the rise in triplet intensity at earlier times. One can see the presence of a shoulder in the experimental signal around 450-550 fs which is we hypothesise is due to the levelling off of the singlet contribution to dissociation and the triplets taking over as the larger contribution to total dissociating population at later times. It is clear that this shoulder in the experimental signal aligns with the change in theoretical singlet and triplet intensities. However, we note that with the current signal to noise ratio and temporal resolution that it is difficult to demonstrate that this shoulder in the signal directly correlated with the change in bulk dissociation channels.

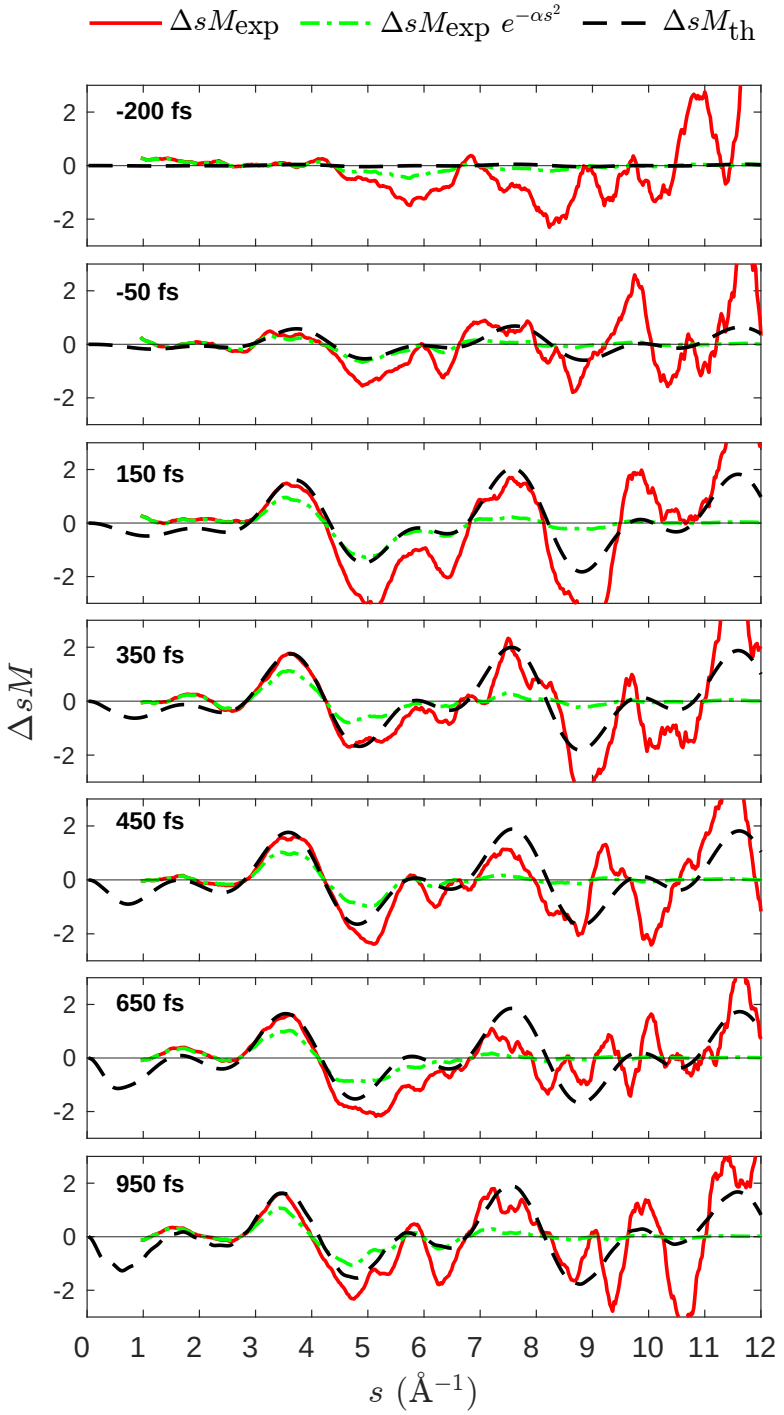

Fig. S1 Comparison of experimental and theoretical ΔsM signal as a function of time. Note the inclusion of the dampened experimental $\Delta sMe^{-\alpha s^2}$ which is transformed into real space to obtain the pair distribution function. The noise at high s is heavily reduced at the risk of reducing the intensity of the signal in the intermediate range. Note the inability of the experimental signal to inaccurately describe the scattered intensity at low values of s.

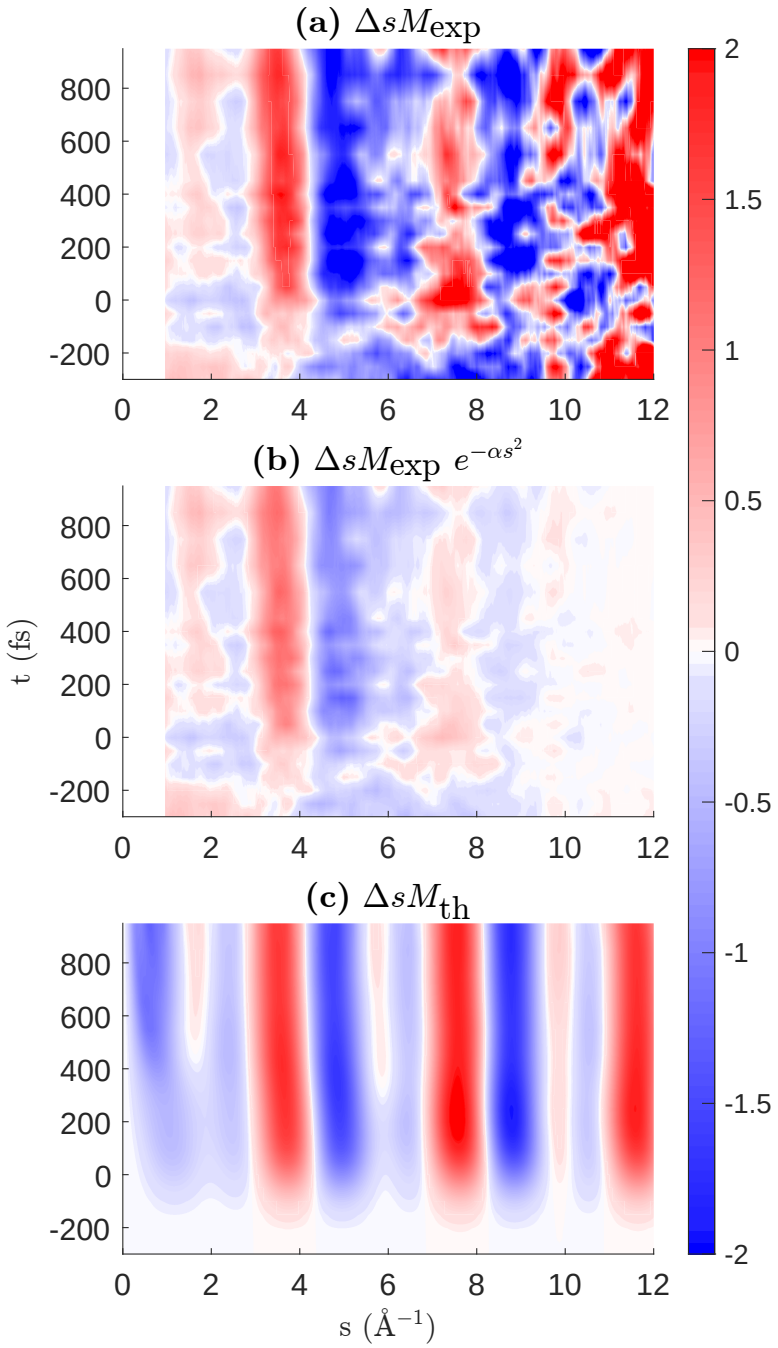

Fig. S2 Heatmaps of a) experimental ΔsM, b) experimental ΔsM weighted by the dampening function, and c) theoretical ΔsM.

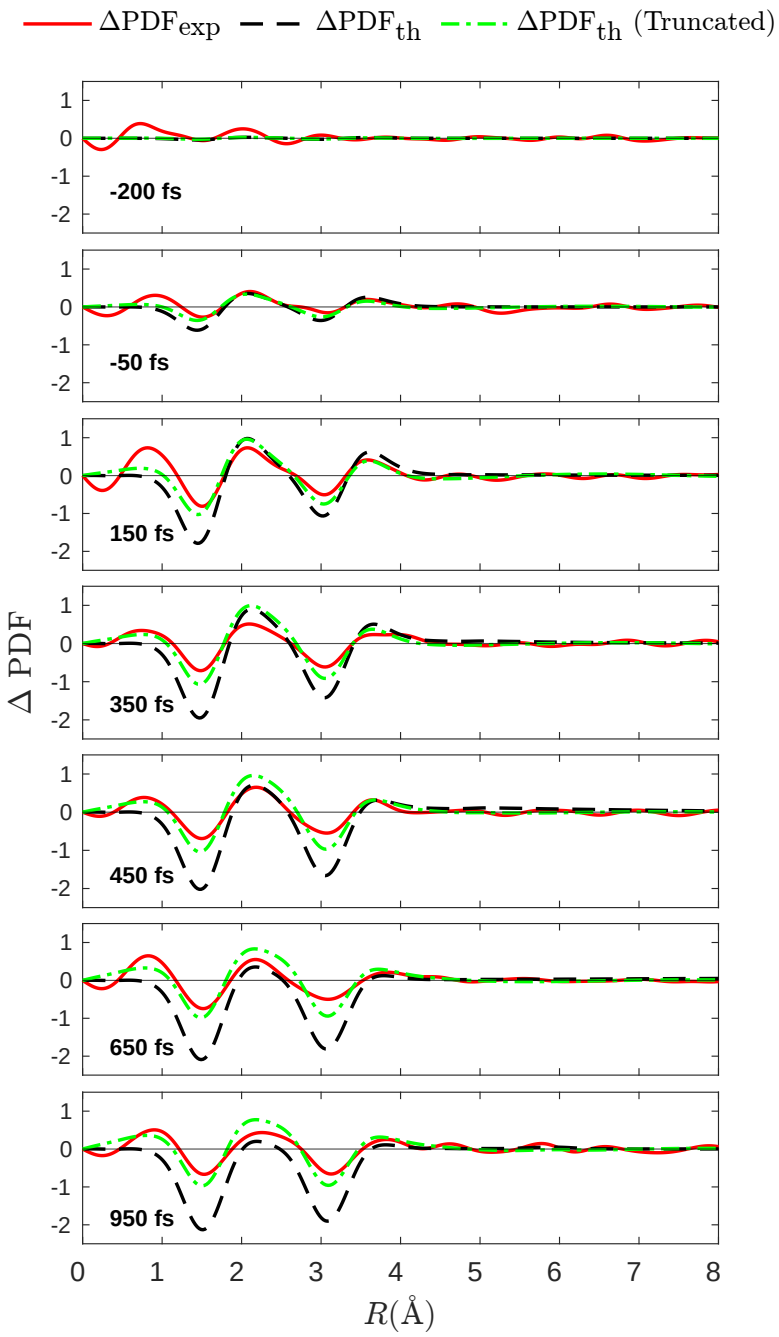

Fig. S3 Lineouts of the experimental and theoretical ΔPDF. Notice that the experiment and the theoretical PDF that results from truncating the transformation range to exclude the low s region show good agreement. The shift in amplitude and the unphysical shoulder at low atomic separations is due to filtering of the low frequencies that make up the signal at low s where the scattered waves are all added coherently as $s \to 0$. The ΔPDF calculated from the theoretical ΔsM that includes the low s data is clearly more physical given the absence of these artifacts.

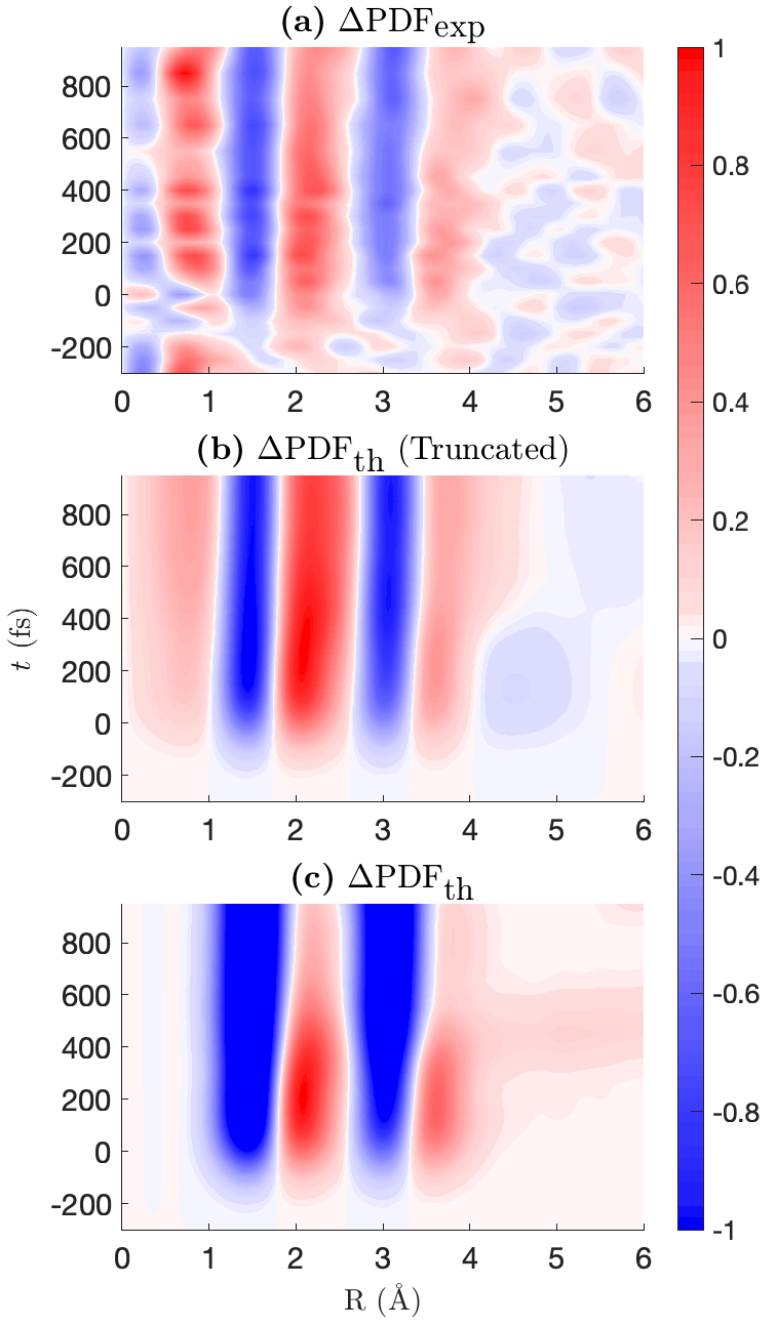

Fig. S4 Heatmaps of a) experimental ΔPDF, b) theoretical ΔPDF calculated over a truncated momentum transfer range, and c) theoretical ΔPDF calculated using the whole available range of momentum transfer.

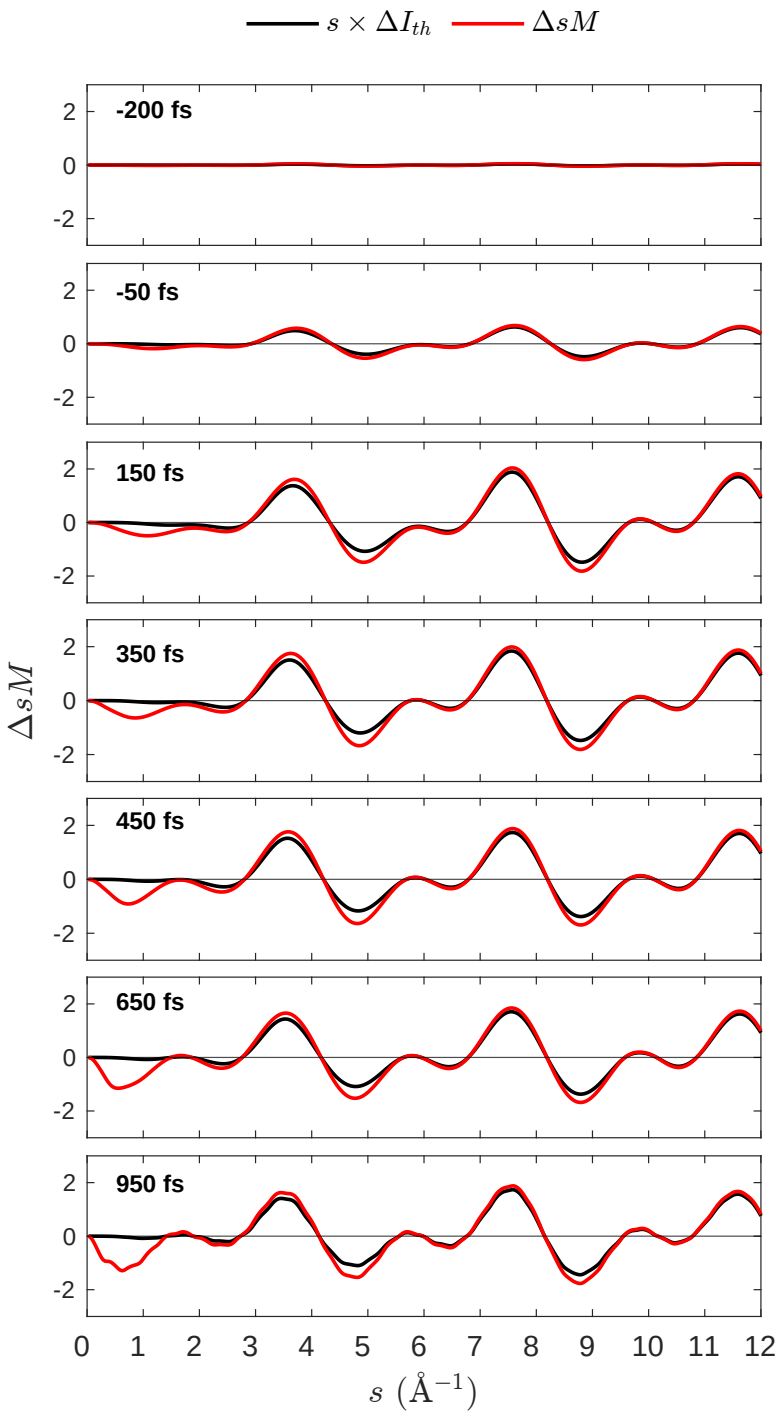

Fig. S5 Comparison of the theoretical signal as calculated using the exact definition of ΔsM and $s \times \%\Delta I$. There is good agreement except at low momentum transfer. One can also see some small deviations that undulate with the local extrema in the signal.

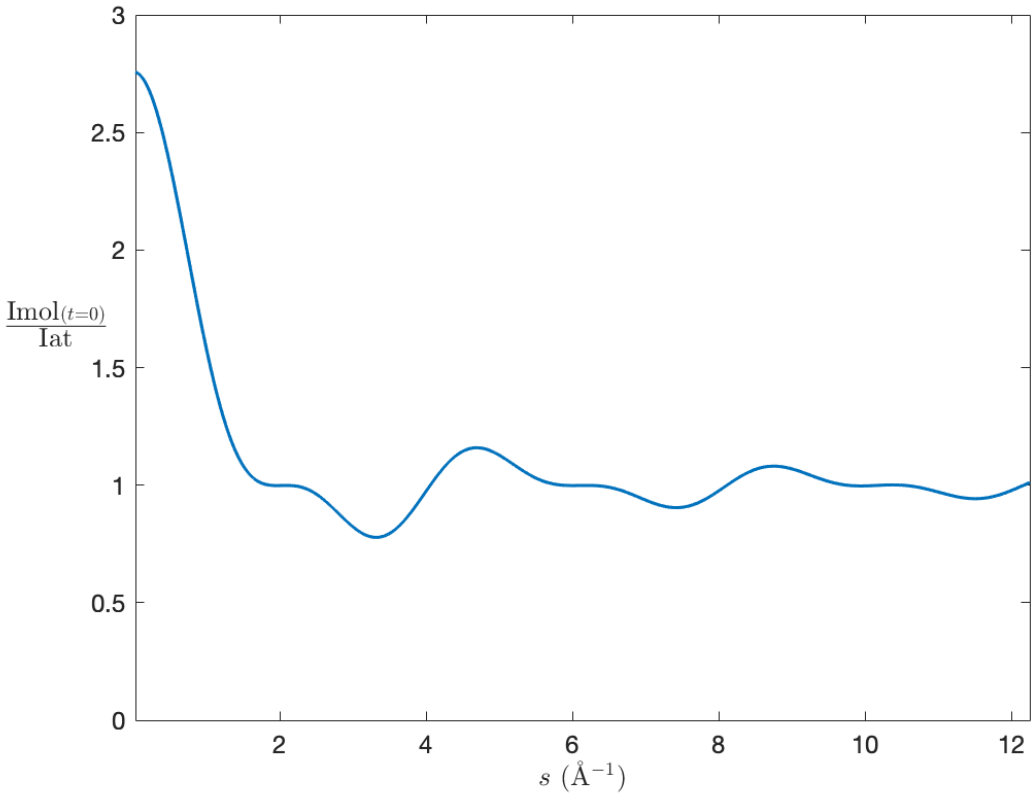

Fig. S6 The ratio of the molecular scattering term for the ground state Wigner distribution (Imol + Iat) vs the atomic scattering term Iat. Note the biggest difference appears at low s with succesivly smaller discrepancies that correspond to the extrema in Fig. S5

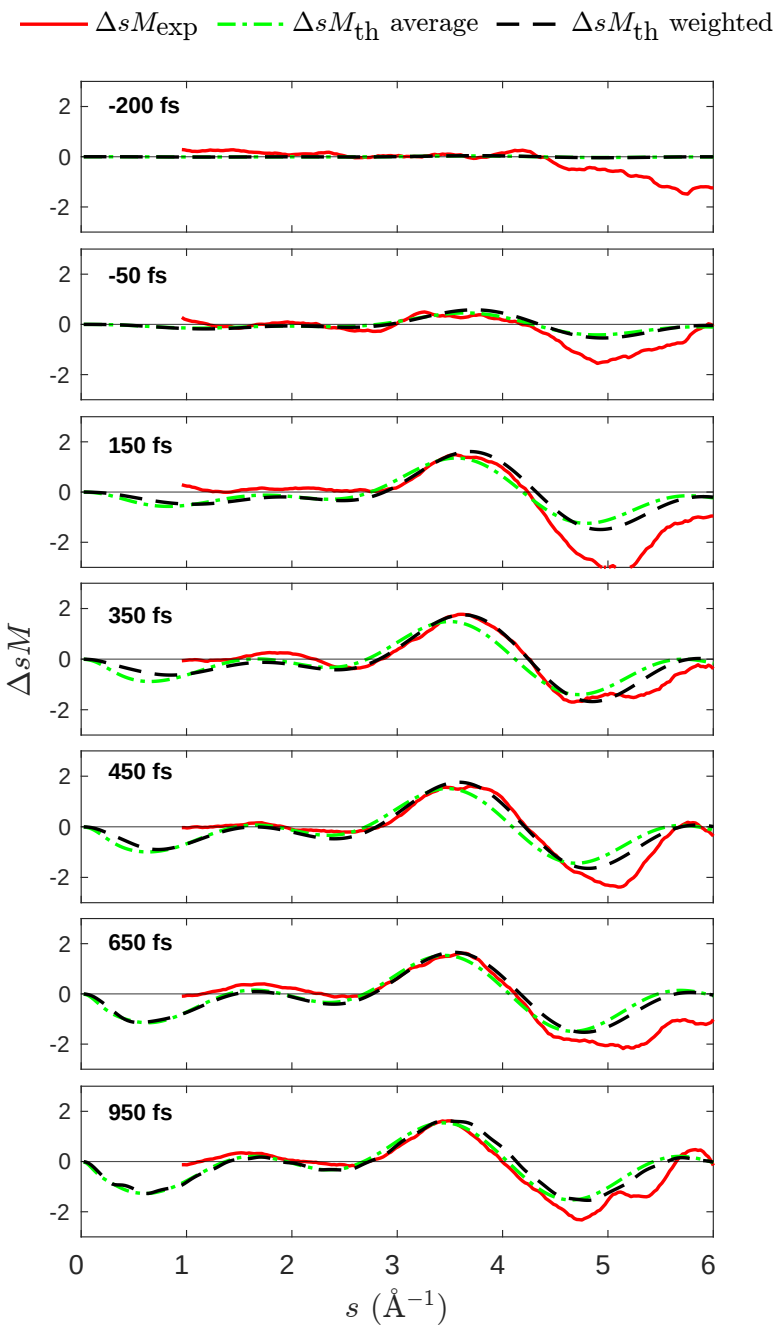

Fig. S7 Comparison of the equally weighted (averaged) theoretical ΔsM with the theoretical ΔsM that results from weighting the signal with the set of weights obtained through the optimisation procedure in the space of $\%\Delta I$. The effect of the weights is subtle, but one can see that the main peak in the region of $3 \leq s \geq 4$ Å^{-1} fits the experimental signal better upon their inclusion.

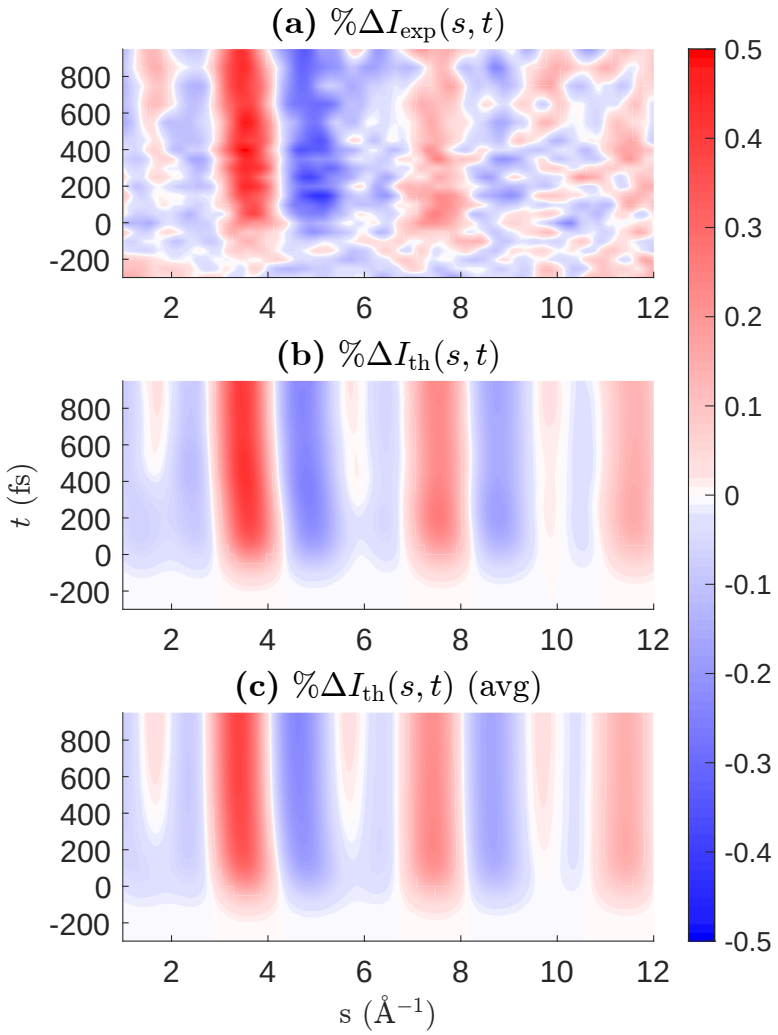

Fig. S8 Heatmaps of a) experimental, b) optimised theoretical, and c) unoptimised (averaged) theoretical scattering signal.

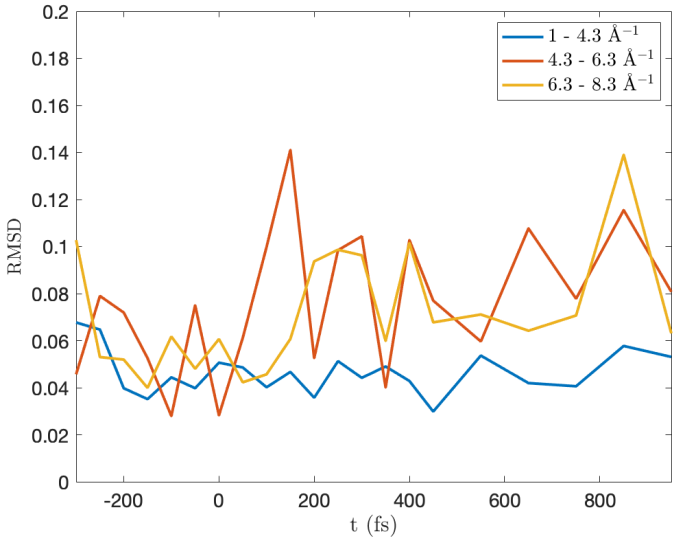

Fig. S9 RMSD calculate for a series of momentum transfer intervals over time. Note the lower RMSD in the low to intermediate s range and the increase in RMSD at higher s.

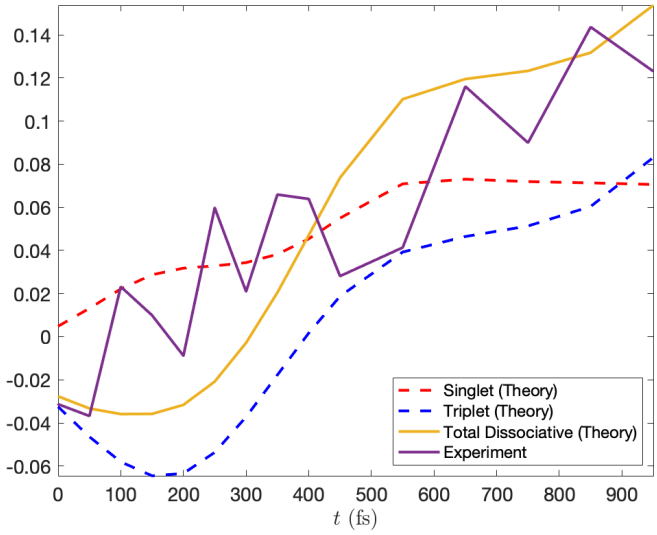

Fig. S10 The total intensity of the centre of the peaks that correspond to the characteristic dissociation signal observed at low s. Plotted are the peak intensities for the singlet and triplet contributions to the theory, as well as the sum of these. One can see the presence of a shoulder in the experimental signal around 450-550 fs which may be the result of the onset of the bulk of the triplet dissociation.